

## Excitation Spectra and Photo-Ionization of Neutral Mercury Centers in Germanium\*

R. A. CHAPMAN AND W. G. HUTCHINSON

*Texas Instruments Incorporated, Dallas, Texas*

(Received 21 November 1966)

The infrared absorption cross section of mercury-doped germanium was measured in wavelength regions in which occur: (1) bound-bound transitions terminating on loosely bound excited states, and (2) photo-ionization to the valence bands. The binding energies of the excited states are quite similar to those observed for the Group III acceptors in germanium. The ground state is split into two levels separated by 0.7 meV. The absorption resonances broaden rapidly above 12°K; lifetime broadening due to phonon absorption is proposed to explain this phenomenon. The integrated absorption cross sections for the resonances predict electric dipole spontaneous lifetimes in the range  $10^{-4}$  to  $10^{-2}$  sec for the bound-bound transitions. The spectral dependence of the photo-ionization cross section can be fitted by a zero-range square-well potential. Photo-ionization to the spin-orbit split-off valence band was observed. There was no evidence for optical-phonon-assisted transitions.

### I. INTRODUCTION

MERCURY-doped germanium has been extensively utilized at temperatures below 30°K as an extrinsic infrared photoconductive detector in the 8–14  $\mu$  region. It is usually prepared by horizontal zone-melting germanium in a high-pressure mercury atmosphere.<sup>1</sup> Like the other Group II acceptors in germanium, the mercury acceptor displays two different ionization energies, depending on the degree of compensation. To a limited extent, these two ionization energies are analogous to the two ionization energies of helium. Similarly, the mercury center displays a number of excited states. The thermal activation energies for the neutral and singly ionized mercury ground states have been observed at 0.087 and 0.23 eV from the valence-band edge.<sup>1</sup>

The purpose of the present work is a thorough examination of the infrared properties of the mercury center and a comparison of the experimental binding energies and experimental photoabsorption cross sections with present theory. Reports of some initial investigations have already been published.<sup>2–4</sup> Other studies of the excited states have also been published recently.<sup>5,6</sup>

### II. THEORY OF DOUBLE ACCEPTORS

At  $k=0$  in germanium, the twofold degenerate valence band belonging to the  $\Gamma_7$  representation of the full double tetrahedral group is spin-orbit split by<sup>7</sup> 0.29

eV from the fourfold degenerate  $\Gamma_8$  light- and heavy-hole valence bands. The ground-state binding energies of all the Group III acceptors in germanium<sup>8,9</sup> are between 0.01047 (boron) and 0.01310 eV (thallium); thus, the spin-orbit splitting of the valence bands is large enough that the ground-state and excited-state binding energies of the Group III acceptors can be predicted by an effective-mass model<sup>10–12</sup> based on Bloch functions from the  $\Gamma_8$  bands only. Similarly, the main features of the neutral mercury center (ground-state binding energy near 0.09 eV) can be explained without the inclusion of the  $\Gamma_7$  valence-band wave functions.

In the effective-mass model, the wave function  $\psi$  of a hole trapped in the Coulombic potential of an acceptor is given by the sum of products of envelope functions  $F_j(r)$  and the fourfold degenerate Bloch functions  $\varphi_j$  for the germanium  $\Gamma_8$  valence bands:

$$\psi(r) = \sum_{j=1}^4 F_j(r) \varphi_j(r).$$

The  $\varphi_j$  Bloch functions transform like atomic  $P_{3/2}$  functions in the vicinity of any lattice point. The functions  $F_j(r)$  approach hydrogenic functions in the limit of parabolic bands. Variational techniques have been used to predict the single-hole binding energies for the various bound states. These states have been classified in terms of the irreducible representation of the full double tetrahedral group and in terms of the parity of the envelope function. Earlier practice favored use of the corresponding atomic notation (1s, 2p, etc.) for the envelope function, but this notation is inaccurate, since the total wave function for a given state can also include small contributions from higher  $l$ -value terms of the same parity. For instance, the ground state of the

\* This work was supported in part by the U. S. Air Force Avionics Laboratory in cooperation with the Advanced Research Projects Agency under Contract No. AF 33(615)-3353.

<sup>1</sup> S. R. Borrello and H. Levinstein, *J. Appl. Phys.* **33**, 2947 (1962).

<sup>2</sup> R. A. Chapman and W. G. Hutchinson, *Solid State Commun.* **3**, 293 (1965).

<sup>3</sup> R. A. Chapman and W. G. Hutchinson, *Bull. Am. Phys. Soc.* **11**, 53 (1966).

<sup>4</sup> R. A. Chapman, W. G. Hutchinson, and T. L. Estle, *Phys. Rev. Letters* **17**, 132 (1966).

<sup>5</sup> B. Pajot and Y. Darvot, *Phys. Letters* **21**, 512 (1966).

<sup>6</sup> W. J. Moore, *Solid State Commun.* **3**, 385 (1965).

<sup>7</sup> E. O. Kane, *J. Phys. Chem. Solids* **1**, 82 (1956).

<sup>8</sup> P. Fisher and H. Y. Fan, *Phys. Rev. Letters* **2**, 456 (1959).

<sup>9</sup> R. L. Jones and P. Fisher, *J. Phys. Chem. Solids* **26**, 1125 (1965).

<sup>10</sup> W. Kohn, in *Solid-State Physics*, edited by F. Seitz and D. Turnbull (Academic Press Inc., New York, 1957), Vol. 5.

<sup>11</sup> D. Schechter, *J. Phys. Chem. Solids* **23**, 237 (1962).

<sup>12</sup> K. S. Mendelson and H. M. James, *J. Phys. Chem. Solids* **25**, 729 (1964).

Group III acceptors in germanium is represented by  $\Gamma_8(+)$  in Schechter's notation<sup>11</sup> or  $(8+0)$  in the notation of Mendelson and James<sup>12</sup> and has an envelope wave function which is largely  $1s$  but which also includes some  $d$  contributions.

The first approximation (valid in the absence of interaction between the holes) for the wave function of the mercury center in its neutral states would be a simple product of the wave functions of the two holes. For this reason, the various states of the mercury center will be identified by double symbols in this paper, e.g.,  $(8+0)^2$ ,  $(8+0)(8-01)$ ,  $(8+0)(8-02)$ , etc. These symbols are sufficient for those excited states of the mercury center in which the two holes have little interaction with each other. The binding energies of these excited states for the Group II acceptor should be expected to be in good agreement with those for the Group III acceptors.

In the  $(8+0)^2$  ground state of the mercury center, it has been shown that the electrostatic interaction between the two  $\Gamma_8$  holes can split this state into two levels.<sup>4</sup> In this case the product representation  $(\Gamma_8 \times \Gamma_8)$  must be reduced to its irreducible forms  $(\Gamma_1 + \Gamma_2 + \Gamma_3 + 2\Gamma_4 + 2\Gamma_5)$ .<sup>13,14</sup> The  $\Gamma_2$ , two  $\Gamma_4$ , and one  $\Gamma_5$  representations can be eliminated because of the Pauli exclusion principle as applied to the coupling of the two  $j = \frac{3}{2}$  holes in the ground state.<sup>4,14,15</sup> In analogy to Hund's rule, the  $\Gamma_3 + \Gamma_5$  ( $j=2$ ) state will be more tightly bound than the  $\Gamma_1$  ( $j=0$ ) state.<sup>15</sup>

### III. EXPERIMENTAL TECHNIQUES

The mercury-doped germanium used in these studies was prepared by a single pass of a melted zone of germanium through a single-crystal germanium sample held in a quartz boat which was enclosed in a sealed quartz capsule containing mercury. A horizontal furnace arrangement similar to that of Borrello and Levinstein<sup>1</sup> was used. The mercury pressure was regulated by a thermocouple placed at the coldest spot of the closed quartz capsule. Mercury pressures up to 20 atm were used. The starting germanium had a net acceptor concentration of almost  $10^{12}/\text{cc}$ . The mercury-doped germanium samples produced were single crystals with dislocation densities of about  $10^8/\text{cm}^2$  on the  $(111)$  face and mercury concentrations of  $10^{15}/\text{cc}$  to  $10^{16}/\text{cc}$  depending on the mercury pressure used during crystal growth.<sup>16</sup> Mercury-doped germanium samples were cut and polished with optically parallel faces separated by either 0.5 or 1.5 cm. The infrared transmission path was always in the  $[111]$  direction.

<sup>13</sup> M. Tinkham, *Group Theory and Quantum Mechanics* (McGraw-Hill Book Company, Inc., New York, 1964).

<sup>14</sup> G. P. Koster *et al.*, *Properties of Thirty-two Point Groups* (MIT Press, Cambridge, Massachusetts, 1964). The notation of this reference is used throughout this present work.

<sup>15</sup> E. V. Condon and G. H. Shortley, *The Theory of Atomic Spectra* (Cambridge University Press, Cambridge, England, 1953).

<sup>16</sup> G. R. Cronin, R. A. Reynolds, and G. B. Larrabee (to be published).

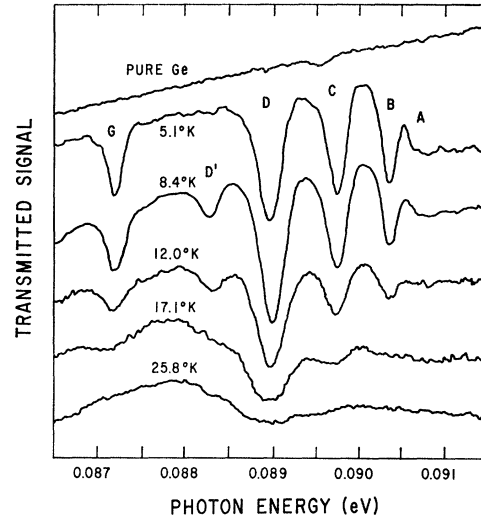


FIG. 1. Infrared transmission through pure germanium and through mercury-doped germanium as a function of temperature in the region of resonant absorption to the excited states. Each signal has been translated vertically for clarity. Sample length = 0.5 cm. Mercury concentration =  $1.1 \times 10^{16}/\text{cm}^3$ .

The mercury concentrations were determined by room-temperature Hall measurements near 22.4 kG. Most of the mercury centers are ionized at room temperature, so that  $N_{\text{Hg}} = r/(eR_H)$ , where  $R_H$  is the measured Hall constant,  $e$  the electronic charge, and  $r$  the Hall correction factor. It was found that 22.4 kG was large enough for the Hall correction factor to be taken as unity.<sup>17</sup>

The incremental absorption coefficient  $\alpha$  due to the mercury center was measured by comparing the transmission of a 0.5-cm-thick mercury-doped germanium sample with 0.5-cm-thick high-purity germanium, thus greatly reducing the effects of reflectivity and lattice absorption. The absorption coefficient  $\alpha$  was determined from the ratio of the signals  $S_{\text{Hg}}/S_{\text{Ge}}$  (where  $S_{\text{Hg}}$  is the signal through the mercury-doped germanium and  $S_{\text{Ge}}$  is the signal through the equal length,  $d$ , pure-germanium sample):

$$(S_{\text{Hg}}/S_{\text{Ge}}) = (1 - \rho^2)e^{-\alpha d} / (1 - \rho^2e^{-2\alpha d}).$$

The reflectivity  $\rho$  was taken as 0.36 for both samples.

Transmission measurements were performed using a Perkin-Elmer model 13U spectrometer with a NaCl prism and a Nernst-glower infrared source. The exit beam from the spectrometer was focused by means of an off-axis parabolic mirror into a jig centered on the bottom of a liquid-helium Cryoflask.<sup>18</sup> The Cryoflask was equipped with KBr windows spaced 180 deg apart, and the Dewar was placed on a stand that could be accurately rotated so that the infrared beam could enter either window. The jig had two  $\frac{3}{16}$ -in.-diam

<sup>17</sup> A. C. Beer and R. K. Willardson, *Phys. Rev.* **110**, 1286 (1958).

<sup>18</sup> Trademark of Texas Instruments.

apertures, each facing one of the KBr windows. A 2 mm×2 mm×6 mm copper-doped germanium photoconductive infrared detector (masked by 1.5-mm-diam aperture) was placed in the center of the jig so that radiation from either aperture would fall on one of the 2 mm by 2 mm faces of the detector. Samples of pure germanium and mercury-doped germanium were placed inside the jig between the two apertures and the detector. The samples were mounted so that no stress could develop as a result of differential thermal contraction. Auxiliary runs with two identical pure-germanium samples established that the copper-doped germanium detector had identical detectivity for either beam direction. A calibrated gallium-doped germanium thermometer was placed in a recess in the copper beneath the mercury-doped germanium sample. The 1.5-cm-long mercury-doped germanium samples (2 mm×2 mm in cross section) were mounted in a different copper jig which had only one aperture and a copper-doped germanium detector.

In the experimental data shown here, carbon dioxide absorption in the light path was greatly reduced by surrounding the region of the light path with plastic and continuously flowing dry nitrogen into the plastic container. On several occasions, carbon dioxide was deliberately introduced to obtain an energy calibration and resolution estimate from the carbon dioxide rotational absorption lines in the 14.5- $\mu$  region.

#### IV. EXCITED STATES

The great difference in the excited-state binding energies (up to 4 meV) compared to the second ionization energy (about 230 meV) indicates there is little overlap between the wave functions of the excited states with 2*p*-like envelope functions and the unexcited 1*s*-like hole. Therefore, the excited states with 2*p*-like envelope functions should be identical in binding energy or energy spacing to those observed in the Group III

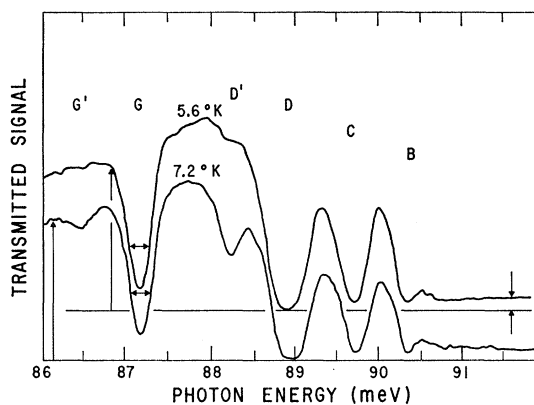


FIG. 2. Infrared transmission in region of photoabsorption resonances for a mercury-doped germanium sample 1.5 cm long and containing about  $1.2 \times 10^{16}/\text{cm}^3$  mercury impurities. The signals have been translated vertically for clarity. The full width at absorption coefficient half-height is shown for the G line.

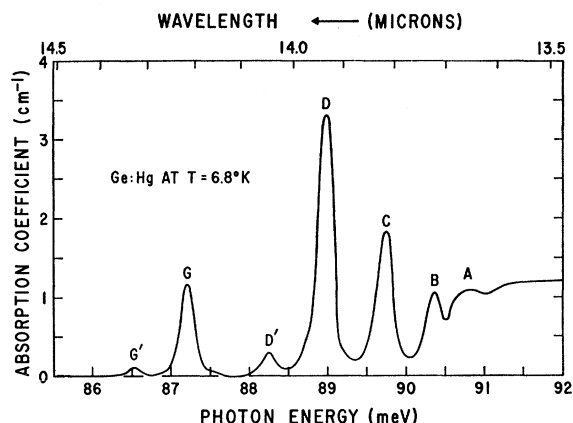


FIG. 3. Photoabsorption coefficient for mercury-doped germanium at 6.8°K in the region of resonant absorption to the excited states. Mercury concentration  $\cong 1.1 \times 10^{16}/\text{cm}^3$ .

acceptors. On the other hand, the 2*s* excited state will be more sensitive to the impurity because 2*s*-like envelope functions have more overlap with a 1*s* envelope function (the unexcited hole). Both expectations were confirmed in this study.

Figure 1 shows the signal detected by the copper-doped germanium detector after the infrared beam has been transmitted through either pure germanium or 0.5-cm-thick mercury-doped germanium containing about  $1.1 \times 10^{16}$  mercury atoms/cm<sup>3</sup>. The vertical scales have been shifted for clarity of presentation. The photoabsorption lines are marked A through G according to the notation of Fisher and Fan.<sup>8</sup> The variation of the photoabsorption spectrum with temperature is shown in this figure. These and similar data are considered in three parts: spectral changes occurring below 10°K (see Figs. 1 and 2), interpretation of the absorption coefficient in terms of the excited states (see Figs. 1, 3, and 4, and Tables I and II) and the dependence of resonance linewidth on temperature (see Figs. 1 and 5).

Figure 2 shows the signal at the copper-doped germanium detector after the infrared beam has been transmitted through a 1.5 cm sample of mercury-doped germanium containing about  $1.2 \times 10^{16}$  mercury atoms/cm<sup>3</sup>. Figures 1 and 2 show that the absorption resonances *D'* and *G'* disappear rapidly toward the lowest temperatures. This was explained earlier<sup>4</sup> as the result of ground-state splitting, with the *D'* and *G'* transitions terminating on the same excited states as the *D* and *G* transitions, respectively. The *D'* and *G'* absorption resonances decrease in intensity because of depopulation of the least-bound initial state. As discussed in Sec. II, the deepest state can be described by a  $\Gamma_3 + \Gamma_5$  representation, while the upper "ground state" can be described by a  $\Gamma_1$  representation. The spontaneous splitting observed between these two states is 0.7 meV and results from the different Coulomb interaction energy between the two holes for the  $\Gamma_1$  and the  $\Gamma_3 + \Gamma_5$  states.

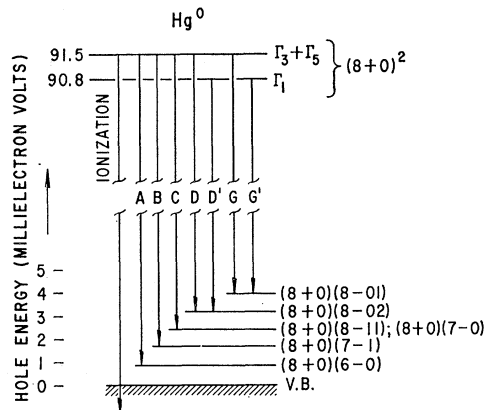


FIG. 4. Correlation of transition energies with bound-state assignments (see text). The valence band is shown at the bottom of the figure.

The best resolution of the absorption lines was obtained below  $10^\circ\text{K}$ . Figure 3 shows the absorption coefficient obtained for a sample 0.5 cm thick containing about  $1.1 \times 10^{16}$  mercury atoms/cm<sup>3</sup> at  $6.8^\circ\text{K}$ . The *A* line is not well resolved in this study because of the high mercury concentration. The resonance energies *A*, *B*, *C*, *D*, *D'*, *G*, and *G'* were measured at 90.8, 90.3, 89.7, 89.0, 88.3, 87.2, and 86.5 meV. These values have been limited to three significant figures because of possible systematic errors in calibration.

Figure 4 shows the correlation between the photoabsorption transitions in the notation *A* through *G* in terms of the ground-state and excited-state notation of Mendelson and James,<sup>12</sup> modified as described in Sec. II for two holes.

Table I shows (1) the energy spacings between the resonances as observed in the present study, (2) results of similar studies by Moore,<sup>6</sup> using a photoconductive technique and a  $1 \times 10^{15}/\text{cm}^3$  mercury concentration, and (3) studies by Pajot and Darvot<sup>5</sup> using a mercury concentration of  $7.3 \times 10^{15}/\text{cm}^3$ . The energy spacings

TABLE I. Ionization energies and energy spacings between absorption transitions in mercury-doped germanium as compared with thallium-doped germanium.<sup>a</sup>

Spacing	Hg This study (meV)	Hg <sup>b</sup> (meV)	Hg <sup>c</sup> (meV)	Tl <sup>a</sup> (meV)
<i>A-D</i>	$1.84 \pm 0.06$	1.74, 1.94	...	1.69, 1.86
<i>B-D</i>	$1.42 \pm 0.05$	$1.42 \pm 0.06$	1.342	1.35
<i>C-D</i>	$0.78 \pm 0.03$	$0.80 \pm 0.06$	0.744	0.75
<i>D-D'</i>	$0.70 \pm 0.04$	$0.67 \pm 0.06$	$0.654^d$	...
<i>D-E</i>	...	...	...	0.74
<i>D-G</i>	$1.79 \pm 0.05$	$1.74 \pm 0.06$	1.695	1.70
<i>G-G'</i>	$0.70 \pm 0.04$	$0.67 \pm 0.06$	$0.606^e$	...
Ionization	$91.5^f \pm 0.02$	...	91.2	13.10

<sup>a</sup> Reference 9.

<sup>b</sup> Reference 6.

<sup>c</sup> Reference 5.

<sup>d</sup> These lines were identified as *E* lines in Refs. 5 and 6 but are reclassified here on the basis of the results of Ref. 4.

<sup>e</sup> These values derived from the unidentified lines of Ref. 5 and the *Z* line of Ref. 5.

<sup>f</sup> This value derived from the present data using the theoretical binding energies of the excited states as predicted in Ref. 12.

quoted for the present work are the average of about 10 runs and, as energy differences, are less sensitive to systematic errors in calibration; therefore, one more significant figure is quoted for these energy differences than for the resonance energies. The mercury lines labeled *E* by other authors have been relabeled *D'* on the basis of the results of Ref. 4. The *D-D'* and *G-G'* spacings are identical within experimental error, in agreement with the assignment of the *D'* and *G'* lines as originating from a ground-state splitting. The results of Jones and Fisher<sup>9</sup> for thallium are also shown, since this Group III acceptor adjoins mercury in the periodic table. The spacings for the mercury lines as measured by the three authors are in agreement within experimental error. The close agreement of the measurements of Pajot and Darvot with the excited states of thallium suggests these measurements are most accurate.

The most loosely bound excited states would be the first to be perturbed by overlap at high mercury concentrations. The *A* line is not well resolved in the present study because of the high mercury concentration used. Using lower concentrations, Moore was able to resolve this line into two lines as seen in the spectra of the Group III acceptors.

Jones and Fisher<sup>9</sup> found that the *2s*-like *E* line moved toward larger binding energies (toward the *G* line) as the ground-state binding energy increased with increasing atomic number. On this basis, the *E* line in mercury-doped germanium could have moved even beyond the *G* line. Several searches out to  $25 \mu$  (42-meV binding energy) were made for additional absorption resonances due to mercury. No additional lines were found, but a weak line would have been hard to detect unless its general position was already known.

The first column of Table II shows the absorption coefficient  $\sigma_j$  integrated over each resonance ( $\Sigma_j = \int \sigma_j dE$ ) in units of  $\text{eV cm}^2$ . One of the features which distinguishes the absorption spectrum of mercury-doped germanium from that of the Group III acceptors is the decreased strength of the *C* line relative to the *D* line. This cannot be wholly described by the near coincidence of the *D* line with a *C'* line which must exist. The line intensity ratios *D/D'* and *G/G'* are both about 10:1. The ratio of degeneracies of the ( $\Gamma_3 + \Gamma_5$ ) state to the  $\Gamma_1$  state is 5:1.

The second column of Table II shows a factor which is proportional to the radiative lifetime for de-excitation of the respective excited state to the ground state by electric dipole emission. The statistical weighting factors of the initial and final states have not been included in this estimate of lifetime. The conditions under which this expression is equal to the radiative lifetime have been discussed by Dexter<sup>19</sup> and by Fowler and Dexter.<sup>20</sup> The requirements are that the ground

<sup>19</sup> D. L. Dexter, in *Solid-State Physics*, edited by F. Seitz and D. Turnbull (Academic Press Inc., New York, 1958), Vol. 6.

<sup>20</sup> W. B. Fowler and D. L. Dexter, *Phys. Rev.* **128**, 2154 (1962).

state and the excited state must experience the same effective electric field and index of refraction  $n$ , the absorption energy and the spontaneous emission energies  $\Delta E_j$  must be equal, and the electric dipole matrix elements between states must be equal for emission and absorption. It is generally presumed that these are good approximations for diffuse impurities in silicon or germanium. The inability of the effective-mass model to predict the ground-state binding energy of the mercury center suggests that the approximations necessary are not rigorous.

Under the same conditions required for the radiative lifetimes to be given by the second column of Table II, the oscillator strengths of the transition are given by  $mc\Sigma_j/(2\pi^2e^2\hbar)$ . For transitions  $B$ ,  $C$ ,  $D$ ,  $D'$ ,  $G$ , and  $G'$  these values are  $3\times 10^{-4}$ ,  $5\times 10^{-4}$ ,  $9\times 10^{-3}$ ,  $8\times 10^{-5}$ ,  $3\times 10^{-4}$ , and  $3\times 10^{-5}$ . Again, the statistical weighting factors for the initial and final states have not been considered.

As the temperature rises above 12°K, all of the resonances begin to broaden very rapidly. The widths of all of the resonances are similar but not necessarily identical. The width of the  $G$  resonance is the only one which is sufficiently isolated to be investigated with confidence; furthermore, the  $D$ ,  $C$ , and  $B$  resonances must be overlapped by  $C'$ ,  $B'$ , and  $A'$  resonances present because of the ground-state splitting. Figure 5 shows the observed width of the  $G$  resonance for the  $1.2\times 10^{16}$  mercury/cc sample of Fig. 2. This full width is measured at half-height of the absorption coefficient which is not the half-height of the transmission dips shown in Fig. 2. This particular run was obtained with 110- $\mu$  slit width (estimated spectral slit width 0.08 meV). The carbon dioxide rotational absorption lines in the region of 14.3  $\mu$  were 0.09 meV wide under the same conditions; this width is shown as "resolution" in the lower left-hand corner of Fig. 5. The widths of the  $G$  resonances shown are *not* corrected for spectrometer "resolution."

One of the possible explanations of the resonance widths is that due to Lax and Burstein<sup>21</sup> who explained the impurity resonant absorption linewidths as being due to acoustic phonons emitted or absorbed during the transition. The phonons are involved because a hole bound in the impurity ground state has a larger interaction with acoustic phonons than does a hole bound in an excited state. The predictions of this theory are very sensitive to the radius  $a$  of the ground state. The zero-temperature width is inversely proportional to the radius squared and this width increases with temperature approximately as  $[\coth\{\Delta/(2T)\}]^{1/2}$ , where  $\Delta=2\hbar v/(ka)$ ,  $v$  is the velocity of sound in the crystal, and  $\hbar$  and  $k$  have their usual meanings. At high temperatures, the widths go asymptotically as  $(2T/\Delta)^{1/2}$ .

The data do not agree with the Lax and Burstein model in two respects: (1) To fit the magnitude of the

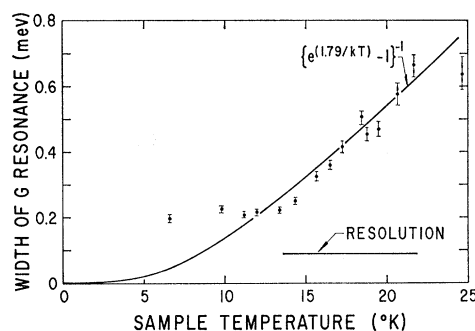


FIG. 5. The temperature dependence of the full width of the  $G$  resonance at half-height of the absorption coefficient for a sample with  $1.2\times 10^{16}$  mercury impurities/cc. The carbon dioxide rotational absorption lines near 14.5  $\mu$  had a width of 0.09 meV when examined with the same spectrometer settings; this width is noted as "resolution" in Fig. 5. The solid line is a theoretical fit for lifetime broadening of the  $G$  line due to transitions to the excited state associated with the  $D$  line caused by acoustic phonon absorption.

width below 12°K, a radius of 50–80 Å is required—this is much too large for the mercury ground state (see Sec. V)—and (2) a plot (not shown) of the width squared versus temperature demonstrates that the increase in width with temperature cannot be fitted by  $\coth\{\Delta/(2T)\}$  for any  $\Delta$ .

Another possible explanation for the resonance widths is lifetime broadening of each excited state due to acoustic phonon absorption and/or emission causing transitions to other excited states. This case has been treated by Kane.<sup>22</sup> He explained the widths of the excited states observed in silicon on the basis of the emission of phonons and a relaxation to a lower excited state. In the examples shown for silicon, Kane's analysis underestimates the widths for the Group III acceptors by about a factor of 30.

In mercury-doped germanium, the  $G$  resonance is the lowest known excited state. There is a possibility that the  $2s$ -like excited state (not observed here) may be

TABLE II. Integrated cross sections ( $\Sigma_j = \int \sigma_j dE$ ) for the photoabsorption resonances and the photo-ionization transitions. The photo-ionization transitions are separated into contributions to the light  $V_1$  and heavy  $V_2$  hole bands ( $\Gamma_8$  bands) and the spin-orbit spin-off  $V_3$  band ( $\Gamma_7$  band). The second column gives a factor proportional to the lifetime for the reverse process of spontaneous radiative decay to the ground state.

Transition	$\Sigma_j$ (eV cm <sup>2</sup> )	$\frac{n^2}{\pi^2\hbar c^2} \left( \frac{\Delta E_j}{\hbar} \right)^2 \Sigma_j$ (sec)
$B$	$0.03\times 10^{-18}$	$2.6\times 10^{-3}$
$C$	$0.05\times 10^{-18}$	$1.5\times 10^{-3}$
$D$	$0.1\times 10^{-18}$	$7.7\times 10^{-4}$
$D'$	$0.009\times 10^{-18}$	$8.5\times 10^{-3}$
$G$	$0.03\times 10^{-18}$	$2.6\times 10^{-3}$
$G'$	$0.003\times 10^{-18}$	$2.6\times 10^{-2}$
$V_1+V_2$	$1.4\times 10^{-16}$	...
$V_3$	$1.0\times 10^{-17}$	...

<sup>21</sup> M. Lax and E. Burstein, Phys. Rev. **100**, 592 (1955).

<sup>22</sup> E. O. Kane, Phys. Rev. **119**, 40 (1960).

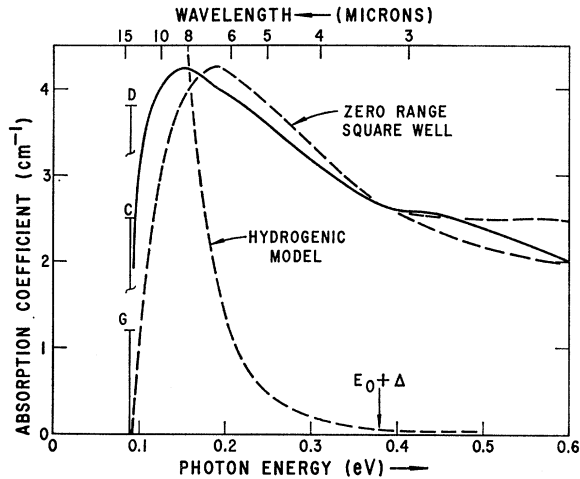


FIG. 6. Photoabsorption coefficient in the region of photo-ionization to the valence bands for a sample containing  $1.1 \times 10^{16}$  mercury/atoms/cm<sup>3</sup>.  $\Delta$  is the 0.29 eV spin-orbit splitting. The theoretical absorption coefficients are shown as dashed curves on the basis of the hydrogenic model of Burstein *et al.* (Ref. 29) and the zero-range square-well model of Lucovsky (Ref. 26). Above 0.38 eV, transitions to the split-off band are predicted on the Lucovsky model for equal effective masses (upper curve) and the known effective masses (lower curve).

more tightly bound than the first  $2p$ -like state (the  $G$  resonance). The data above 12°K however can be interpreted on the basis of observed excited states if absorption of phonons and transition to the second  $2p$ -like excited state (the  $D$  resonance) is considered. The prediction for lifetime broadening due to phonon absorption from the first known excited state (4-meV binding energy) to the second known excited state 1.79 meV higher is<sup>22</sup>

$$\Delta E = 3.8 \times 10^{-2} \{ \exp(20.8/T) - 1 \}^{-1} \text{ meV},$$

where the constant was derived using the known constants for germanium, a deformation potential of 15 eV as used by Kane, and an excited-state radius of 60 Å for both excited states. The solid line in Fig. 5 shows this expression for a constant of 1.0 rather than  $3.8 \times 10^{-2}$ . This substitution is in line with prior observations that this model underestimates the minimum width by about a factor of 30. Thus, the temperature dependence of the data above 12°K fits the model of lifetime broadening by phonon absorption better than any other, but the lack of quantitative agreement prevents a definitive conclusion.

The proposed lifetime broadening due to absorption of phonons would cause a hopping of carriers up the ladder of excited states in the opposite sense to the cascading process in the giant trap mechanism proposed by Lax<sup>23,24</sup> to explain free-carrier capture cross sections of ionized impurities. The higher excited states will be affected by phonon emission as well as absorption.

The 0.2-meV width below 12°K must be explained by some other mechanism. This width could be due to the sum of a number of contributions such as phonon emission to an otherwise undetected  $2s$  excited state, transitions to the ground state which is broadened by a mechanism similar to that proposed by Lax and Burstein, or residual stress splitting of the excited states.

## V. PHOTO-IONIZATION

The photo-ionization threshold, or optical activation energy, of the neutral mercury center can be most accurately determined as the series limit of the excited-state resonances. To do this, the theoretical binding energy<sup>11,12</sup> of each state is added to the resonance energy and these sums are averaged for all states. The last row in Table I shows the photo-ionization threshold of  $91.5 \pm 0.2$  meV so derived, using the predictions of Mendelson and James<sup>12</sup> to be consistent with the results of Jones and Fisher<sup>9</sup> for the Group III acceptors. Alternate use of the binding energies of Schechter<sup>11</sup> lowers the extrapolated threshold by 0.3 meV.

The photo-ionization absorption cross section for the neutral mercury acceptor in germanium is shown in Fig. 6 for a mercury concentration of  $1.1 \times 10^{16}$ /cm<sup>3</sup>. The energy dependence of the photo-ionization cross section will depend on the potential binding the hole to the acceptor; that is, the cross section will be determined by the wave functions of the initial and final states.

The cross sections for photo-ionization shown in Fig. 6 can be integrated over energy for the light  $V_1$  and heavy  $V_2$  hole bands separately from the spin-orbit split-off band. These integrated cross sections ( $0 < h\nu < 0.6$  eV) are shown at the bottom of Table II. The sum of photoexcitation and photo-ionization oscillator strengths (under the assumptions of Sec. IV) is 1.4 and this can be increased to 2.0 if the data are extrapolated above photon energies of 0.6 eV. This agrees with the  $f$ -value sum-rule value of 2 for an atom with two bound electrons<sup>25</sup> for an effective electric field ratio of unity (see Sec. IV).

Since the mercury center is much more tightly bound than would be expected for a two-hole center bound by a Coulomb potential, some short-range perturbation must be affecting the potential. Lucovsky<sup>26</sup> has used the zero-range square-well potential model developed for nuclear photodisintegration of deuterium to predict the photo-ionization cross section  $\sigma$  for Group III deep acceptors in silicon:

$$\sigma = \left[ \left( \frac{E_{\text{eff}}}{E_0} \right)^2 \frac{1}{n(m^*/m)} \right] \frac{16\pi e^2 h E_I^{1/2} (h\nu - E_I)^{3/2}}{3mc (h\nu)^3},$$

where  $E_{\text{eff}}/E_0$  is the effective field ratio,<sup>19</sup>  $n$  the index of refraction,  $m^*$  the effective mass of the bound carrier,

<sup>23</sup> M. Lax, *J. Phys. Chem. Solids* **8**, 66 (1959).

<sup>24</sup> M. Lax, *Phys. Rev.* **119**, 1502 (1960).

<sup>25</sup> H. G. Kuhn, *Atomic Spectra* (Academic Press Inc., New York, 1962).

<sup>26</sup> G. Lucovsky, *Solid State Commun.* **3**, 299 (1965).

and  $E_I$  the threshold energy. All the other symbols have their usual meanings. This formula includes the effect of two holes and unpolarized light.<sup>27</sup> Figure 6 shows this zero-range model fitted to the data for mercury-doped germanium for  $(E_{\text{eff}}/E_0)=1.2$ , which results in equal magnitude maximum. This value of effective field ratio is reasonable for a relatively diffuse center.<sup>19</sup> The good fit of the sum of oscillator strengths to the  $f$ -value sum rule for  $(E_{\text{eff}}/E_0)=1.0$  strengthens this conclusion.

The Lucovsky model predicts that the cross section will peak at 183 meV. The experimental data of Fig. 6 peak at 150 meV which is 82% of the theoretical prediction. The Lucovsky model also predicts that the cross section goes to zero at threshold. The data of Fig. 6 show a cross section at threshold which is nearly 50% of the peak value.

The data of Fig. 6 also show another increase in cross section near 370 meV, which is the result of transitions to the spin-orbit split-off  $\Gamma_7$  valence band. The model of Lucovsky can be modified to include this effect; the major uncertainty is the ratio of effective masses in the bound state and the  $\Gamma_7$  band. The dashed curves for the zero-range potential in Fig. 6 show the predictions for a spin-orbit splitting of 0.29 eV and for (1) equal masses and (2) masses given by a bound hole mass of  $0.3 m_0$  and a mass of  $0.077 m_0$  in the split-off band.

The potential binding the mercury center is ultimately of electrostatic origin. If one assumes a Coulomb potential and neglects the interaction between the two holes, a simple modification of the cross section  $\sigma$  for photo-ionization of a hydrogenic atom<sup>28,29</sup> may be used as an alternate model. An extra factor of 2 has to be included to count both holes bound on the mercury center.<sup>28</sup> This theoretical cross section is shown in Fig. 6 as the hydrogenic approximation for  $(E_{\text{eff}}/E_0)=1.2$ . This is the same effective field ratio used for the fit to the Lucovsky model. The hydrogenic model is not in good agreement with experiment, and the shift to a more correct helium-like model<sup>28</sup> in a pure Coulombic field would not be expected to greatly improve the agreement.

The shape of the photo-ionization cross section shown in Fig. 6 is not unique to the Lucovsky model. Bebb<sup>30</sup> has recently shown that the photo-ionization cross sections for the Group III acceptors in silicon can be derived more accurately using quantum-defect techniques.<sup>31</sup> Studies are now underway using this technique and the inclusion of many-body effects.

<sup>27</sup> J. M. Blatt and V. F. Weisskopf, *Theoretical Nuclear Physics* (John Wiley & Sons, Inc., New York, 1952).

<sup>28</sup> H. A. Bethe and E. E. Salpeter, in *Handbuch der Physik*, edited by S. Flügge (Springer-Verlag, Berlin, 1957), Vol. XXXV, p. 88.

<sup>29</sup> E. Burstein, G. Picus, and N. Sclar, *Photoconductivity Conference* (John Wiley & Sons, Inc., New York, 1956), p. 353.

<sup>30</sup> H. B. Bebb, *Bull. Am. Phys. Soc.* **12**, 342 (1967).

<sup>31</sup> A. Burgess and M. J. Seaton, *Monthly Notices Roy. Astron. Soc.* **120**, 121 (1960).

A search near 0.38 eV was made for photoabsorption resonances due to transitions to excited states associated with the spin-orbit split-off valence band.<sup>32</sup> No resonances could be detected, but such resonances could be masked by the cross section for photo-ionization to the light- and heavy-hole band which is still appreciable just below the 0.38 (=0.29+0.09) eV threshold. Likewise, no resonances could be detected associated with optical-phonon-assisted bound-bound transitions as have been observed for diamond.<sup>33</sup>

No anomalies in the photoabsorption cross section were detected<sup>34</sup> which could be correlated with optical-phonon-assisted photo-ionization. This suggests that the oscillatory photoconductivity observed for zinc- or copper-doped germanium<sup>35</sup> is due in large part to optical phonon effects on transport or free-carrier recombination parameters as is the case in intrinsic photoconductivity.<sup>36,37</sup>

## VI. SUMMARY

The 91.5-meV photo-ionization threshold of the neutral mercury ground state is several times larger than the first-order estimate of 20 meV for the ionization threshold<sup>38</sup> for a two-hole acceptor based on the binding energies of the single-hole Group III acceptors in germanium. The wavelength dependence of the photo-ionization cross section provides experimental verification that the potential has been greatly perturbed from Coulombic at small distances from the mercury impurity. The general features of these data can be fit by the zero-range square-well potential of Lucovsky.<sup>26</sup> The magnitude of the photo-ionization cross section is in agreement with the Lucovsky model for an effective electric field ratio  $(E_{\text{eff}}/E_0)$  near unity as expected for a diffuse center<sup>19</sup>;  $(E_{\text{eff}}/E_0) \cong 1$  also makes the  $f$ -value sum (derived from the integrated cross sections) approximately 2 as required for a center with two bound particles.<sup>25</sup> The Lucovsky model does not accurately predict the energy at which the maximum photo-ionization cross section occurs. Furthermore, the experimental cross section does not go to zero at threshold.

In addition to photo-ionization to the light- and heavy-hole valence bands, photo-ionization is observed to the spin-orbit split-off valence band with a threshold

<sup>32</sup> S. Zwerdling, K. J. Button, B. Lax, and L. M. Roth, *Phys. Rev. Letters* **4**, 173 (1960).

<sup>33</sup> S. D. Smith and W. Taylor, *Proc. Phys. Soc. (London)* **79**, 1142 (1962).

<sup>34</sup> The small anomalies seen in the data of Ref. 2 were due to uncorrected atmospheric absorption.

<sup>35</sup> C. Benoit a la Guillaume and J. Cernogora, *J. Phys. Chem. Solids* **24**, 383 (1963).

<sup>36</sup> M. A. Habegger and H. Y. Fan, *Phys. Rev. Letters* **12**, 99 (1964).

<sup>37</sup> H. J. Stocker, C. R. Stannard, Jr., H. Kaplan, and H. Levinstein, *Phys. Rev. Letters* **12**, 163 (1964).

<sup>38</sup> A. Glodeanu, *Phys. Letters* **14**, 268 (1965). The estimate 20 meV given in the present text is based on an effective mass of  $0.2 m_0$  while Glodeanu used  $1.0 m_0$  for double donors.

near 0.381 meV (0.290+0.091 meV). No effects due to optical-phonon-assisted transitions were observed.

Within experimental error, most of the excited states of the neutral mercury center are the same as those observed for the single-hole Group III acceptors in germanium. This observation shows that at large distances (greater than 100 Å) the potential provided by the singly ionized mercury center is identical to that provided by a singly ionized Group III acceptor. The exception to the agreement of the excited states is that the  $2s$ -like ( $\{8+0\}\{8+1\}$ ) state<sup>9,12</sup> is not observed; this state is expected to be more sensitive to the short-range perturbation. The integrated cross sections for the photoexcitation resonances predict electric dipole spontaneous decay lifetimes of the order of  $10^{-4}$  to  $10^{-2}$  sec.

Below 10°K, two photoexcitation resonances disappear. These resonances are satellites to the  $D$  and  $G$  resonances and are separated from these resonances by 0.7 meV. The only possible explanation for this phenomenon is that the neutral ground state is split by 0.7 meV. This splitting has been explained on the basis of the electrostatic interaction between the two bound holes.<sup>4</sup>

The temperature dependence of the resonance linewidths was studied using the  $G$  resonance which was well separated from the other resonances. Below 10°K, the full width at half-height of the absorption coefficient was 0.2 meV when the instrumental resolution was near 0.09 meV. No one theory can be used to explain all the data using observed excited states. However, above

10°K the temperature dependence of the resonance width can be explained on the basis of lifetime broadening<sup>22</sup> due to phonon absorption and transition to the excited state 1.79 meV as above that state causing the  $G$  resonance. Below 10°K, the magnitude of the temperature-independent resonance width requires a large ground-state width (the Lax and Burstein mechanism<sup>24</sup> or residual strains) or lifetime broadening<sup>22</sup> of the first-excited state due to phonon emission to a more tightly bound excited state (the  $2s$ -like state) not yet observed in photoabsorption for mercury-doped germanium.

*Note added in proof:* Since this paper was submitted, photo-ionization cross sections for deep acceptors including the neutral mercury double-acceptor in germanium have been predicted using the more rigorous quantum-defect calculations. The experimental data of Fig. 6 are in good agreement with predictions. [H. B. Bebb and R. A. Chapman (to be published).]

#### ACKNOWLEDGMENTS

The authors wish to thank T. L. Estle, H. B. Bebb, and W. C. Scott for useful discussions and suggestions concerning this work. Special thanks are due to T. L. Estle who had the major part in the theoretical explanation of the ground-state splitting first reported in an earlier publication. The authors are also grateful to G. R. Cronin for the mercury-doped germanium samples used in this study and to R. A. Reynolds for Hall measurements and useful discussions.